What is a 'Hard' Process?

'Hard' processes have a large scale in the calculation that makes perturbative QCD applicable: high momentum transfer, Q^2, high invariant mass, M, high transverse momentum, p_T

Understanding these processes relies on asymptotic freedom to calculate the interactions between two hadrons on the quark/gluon level but the confinement scale determines the probability of finding a particular parton in the proton

This implies factorization between the perturbative hard part and the universal, nonperturbative parton distribution functions

$$\sigma_{AB}(s,m_Q^2) = \sum_{i,j=q,\bar{q},g} \int_{4m_Q^2/s}^1 \frac{d\tau}{\tau} \int dx_1\, dx_2\, \delta(x_1x_2-\tau) \times F_i^A(x_1,\mu^2)\, F_j^B(x_2,\mu^2)\, \hat{\sigma}_{ij}(\tau,m_Q^2,\mu^2)$$

F_i^A are the parton distributions, either in a proton or a nucleus, determined from fits to data, x_1 and x_2 are the fractional momentum of the hadron carried by partons i and j

$\hat{\sigma}_{ij}(\tau,m_Q^2,\mu^2)$ is partonic cross section calculable in QCD in powers of α_s^{2+n}: leading order, $n=0$; next-to-leading order, $n=1$ ...

Studying the Nuclear Gluon Distribution in pA

Lepton pairs from heavy quark decays used to compare the pA/pp ratios at the same energy to the input shadowing parameterization

$c\bar{c}$ and $b\bar{b}$ pairs produced, hadronized, and decayed, then studied in the PHENIX and ALICE lepton pair acceptances

Both correlated and uncorrelated pairs considered

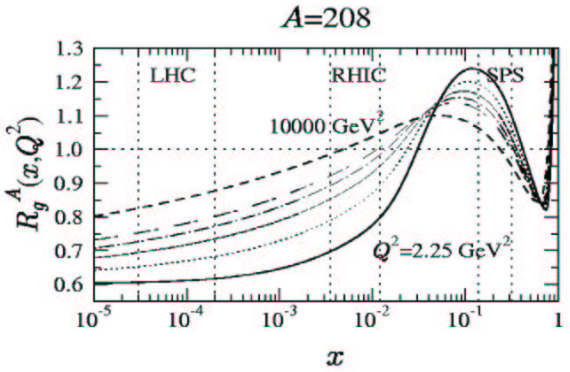

Figure 8: Scale evolution of the EKS98 ratio $R_g^A(x,Q^2)$ for A=208. The ratios are shown as functions of x at fixed values of Q^2 equidistant in $\log Q^2$: 2.25 GeV² (solid), 5.39 GeV² (dotted), 14.7 GeV² (dashed), 39.9 GeV² (dotted-dashed), 108 GeV² (double-dashed), and 10000 GeV² (dashed). The regions between the vertical dashed lines show the dominant values of x_2 probed by muon pair production from $D\overline{D}$ at SPS, RHIC and LHC energies. [K.J. Eskola, V.J. Kolhinen and R.V., Nucl. Phys. **A696** (2001) 729.]

Lepton Pair Cross Section

Differential cross section

$$\frac{d\sigma^{pA\to l\bar{l}+X}}{dM_{l\bar{l}}dy_{l\bar{l}}} = \int d^3\vec{p}_l d^3\vec{p}_{\bar{l}} \int d^3\vec{p}_H d^3\vec{p}_{\overline{H}}\, \delta(M_{l\bar{l}} - M(p_l,p_{\bar{l}}))\, \delta(y_{l\bar{l}} - y(p_l,p_{\bar{l}}))$$
$$\times \frac{d\Gamma^{H\to l+X}(\vec{p}_H)}{d^3\vec{p}_l}\, \frac{d\Gamma^{\overline{H}\to \bar{l}+X}(\vec{p}_{\overline{H}})}{d^3\vec{p}_{\bar{l}}}\, \frac{d\sigma^{pA\to H\overline{H}+X}}{d^3\vec{p}_H d^3\vec{p}_{\overline{H}}}$$
$$\times\theta(y_{\min} < y_l, y_{\bar{l}} < y_{\max})\theta(\phi_{\min} < \phi_l, \phi_{\bar{l}} < \phi_{\max})$$

Decay rate is $d\Gamma^{H\to l+X}(\vec{p}_H)/d^3\vec{p}_l$ for meson H to decay to lepton

Theta functions define rapidity and ϕ cuts

$M_{l\bar{l}}$ and $y_{l\bar{l}}$ are the mass and the rapidity of the lepton pair

$$M(p_l,p_{\bar{l}}) = \sqrt{(p_l+p_{\bar{l}})^2}\,,$$
$$y(p_l,p_{\bar{l}}) = \frac{1}{2}\ln\left(\frac{(E_l+E_{\bar{l}})+(p_{lz}+p_{\bar{l}z})}{(E_l+E_{\bar{l}})-(p_{lz}+p_{\bar{l}z})}\right)$$

Meson pair production cross section

$$\frac{d\sigma^{pA\to H\overline{H}+X}}{d^3\vec{p}_H d^3\vec{p}_{\overline{H}}} = \int \frac{d^3\vec{p}_Q}{E_Q}\frac{d^3\vec{p}_{\overline{Q}}}{E_{\overline{Q}}} E_Q E_{\overline{Q}} \frac{d\sigma^{pA\to Q\overline{Q}+X}}{d^3\vec{p}_Q d^3\vec{p}_{\overline{Q}}} \int_0^1 dz_1 D_Q^H(z_1) \int_0^1 dz_2 D_{\overline{Q}}^{\overline{H}}(z_2)$$
$$\times\ \delta^{(3)}(\vec{p}_H - z_1\vec{p}_Q)\,\delta^{(3)}(\vec{p}_{\overline{H}} - z_2\vec{p}_{\overline{Q}})$$

Hadronic Heavy Quark Production Cross Section per Nucleon

$$\frac{1}{A}E_Q E_{\overline{Q}}\frac{d\sigma^{pA\to Q\overline{Q}+X}}{d^3\vec{p}_Q d^3\vec{p}_{\overline{Q}}} = \sum_{i,j}\int_0^1 dx_1 \int_0^1 dx_2\, f_i^p(x_1,Q^2) f_j^A(x_2,Q^2) E_Q E_{\overline{Q}}\frac{d\hat{\sigma}^{ij\to Q\overline{Q}}}{d^3\vec{p}_Q d^3\vec{p}_{\overline{Q}}}$$

Parton distribution functions in proton, f_i^p, and nucleus, $f_j^A = f_j^p R_j^A$, evaluated at $Q^2 \propto m_{T_Q}^2$

Partonic cross sections and convolution of parton distributions with subprocess cross sections

$$E_Q E_{\overline{Q}}\frac{d\hat{\sigma}^{ij\to Q\overline{Q}}}{d^3\vec{p}_Q d^3\vec{p}_{\overline{Q}}} = \frac{\hat{s}}{2\pi}\frac{d\hat{\sigma}^{ij\to Q\overline{Q}}}{d\hat{t}}\delta^{(4)}(p_1+p_2-p_Q-p_{\overline{Q}})$$

$$\sum_{i,j} f_i^p(x_1,Q^2) f_j^A(x_2,Q^2)\frac{d\hat{\sigma}^{ij\to Q\overline{Q}}}{d\hat{t}} = \frac{1}{16\pi\hat{s}^2}\Big(f_g^p(x_1,Q^2) f_g^A(x_2,Q^2)\overline{|\mathcal{M}_{gg\to Q\overline{Q}}|^2}$$
$$+ \sum_{q=u,d,s}[f_q^p(x_1,Q^2) f_{\bar{q}}^A(x_2,Q^2) + f_{\bar{q}}^p(x_1,Q^2) f_q^A(x_2,Q^2)]\overline{|\mathcal{M}_{q\bar{q}\to Q\overline{Q}}|^2}\Big)$$

Differential and total cross sections per nucleon

$$\frac{d\tilde{\sigma}^{Q\overline{Q}}}{d^3\vec{p}_Q d^3\vec{p}_{\overline{Q}}} = \frac{1}{E_Q}\frac{1}{E_{\overline{Q}}}\left[\frac{1}{A}E_Q E_{\overline{Q}}\frac{d\sigma^{pA\to Q\overline{Q}+X}}{d^3\vec{p}_Q d^3\vec{p}_{\overline{Q}}}\right]$$
$$\tilde{\sigma}^{Q\overline{Q}} = \int d^3\vec{p}_Q\, d^3\vec{p}_{\overline{Q}}\frac{d\tilde{\sigma}^{Q\overline{Q}}}{d^3\vec{p}_Q d^3\vec{p}_{\overline{Q}}}$$
$$= \int dp_T^2 dy_1 dy_2 \sum_{ij} x_1 f_i^p(x_1,Q^2) x_2 f_j^A(x_2,Q^2)\frac{d\hat{\sigma}^{ij\to Q\overline{Q}}}{d\hat{t}}$$

Ratios of Lepton Pairs in the e^+e^- and $\mu^+\mu^-$ Channels

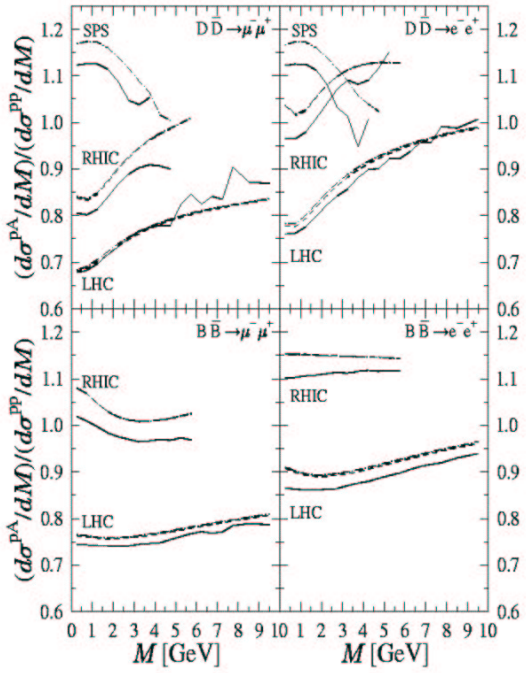

Figure 9: The ratios of lepton pairs from correlated $D\overline{D}$ and $B\overline{B}$ decays in pA to pp collisions at the same energies (solid curves). Both the e^+e^- and $\mu^+\mu^-$ channels are shown. The results are compared to the input nuclear gluon distribution from EKS98 at the average x_2 and Q (dashed)/$\sqrt{\langle Q^2\rangle}$ (dot-dashed) of each M bin. [K.J. Eskola, V.J. Kolhinen and R.V., Nucl. Phys. **A696** (2001) 729.]

Why Don't the Results Match the Input Exactly?

Some production is through the $q\overline{q}\to Q\overline{Q}$ channel which has different shadowing

Better agreement at LHC because of reduced $q\overline{q}$ contribution

Phase space integration smears the shadowing relative to R_g^A evaluated at the average values of x_2 and Q

Curvature of R_g^A with x stronger at large x

Average values of x_2 of target is larger for electrons (forward muon coverage allows smaller x_2's to be reached) so the deviations between the output and input are largest in the central coverages of the electron detectors

Average Values of x_2 and Q

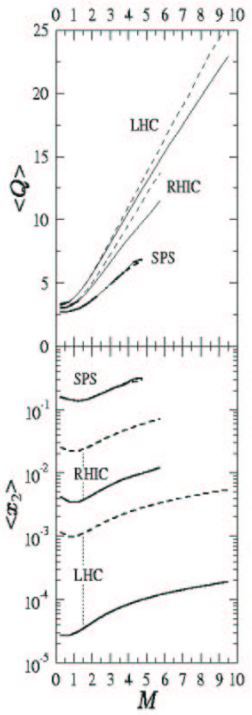

Figure 10: The average values of x_2 and Q are given as a function of lepton pair mass for $D\overline{D}$ decays. The solid lines are for muon pairs while the dashed are for electron pairs. The dotted lines on the average x_2 plot indicate the difference between the channels. [K.J. Eskola, V.J. Kolhinen and R.V., Nucl. Phys. **A696** (2001) 729.]

Correlated and Uncorrelated Decays

Impact parameter integrated cross section

$$\sigma^{pA\to Q\overline{Q}+X} = \int d^2\mathbf{b}\,(1-e^{-T_A(\mathbf{b})\tilde{\sigma}^{Q\overline{Q}}}) = \int d^2\mathbf{b}\sum_{N=1}^{\infty}\frac{\overline{N}^N_{Q\overline{Q}}(\mathbf{b})e^{-\overline{N}_{Q\overline{Q}}(\mathbf{b})}}{N!}$$

Number of $Q\overline{Q}$ pairs at impact parameter b proportional to thickness function

$$\begin{aligned}\overline{N}_{Q\overline{Q}}(\mathbf{b}) &= T_A(\mathbf{b})\tilde{\sigma}^{Q\overline{Q}}\\ T_A(\mathbf{b}) &= \int dz\rho_A(\mathbf{b},z)\end{aligned}$$

Differentiating:

$$\begin{aligned}\frac{d\sigma^{pA\to Q\overline{Q}+X}}{d^3\vec{p}_Q d^3\vec{p}_{\overline{Q}}} &= \int d^2\mathbf{b}\sum_{N=1}^{\infty}\frac{\overline{N}^N_{Q\overline{Q}}(\mathbf{b})e^{-\overline{N}_{Q\overline{Q}}(\mathbf{b})}}{N!}\prod_{i=1}^{N}\Big(\frac{1}{\tilde{\sigma}^{Q\overline{Q}}}\int d^3\vec{p}_{Qi}d^3\vec{p}_{\overline{Q}i}\frac{d\tilde{\sigma}^{Q\overline{Q}}}{d^3\vec{p}_{Qi}d^3\vec{p}_{\overline{Q}i}}\Big)\\ &\times\Big(\sum_{j,k=1}^{N}\delta^{(3)}(\vec{p}_Q-\vec{p}_{Qj})\delta^{(3)}(\vec{p}_{\overline{Q}}-\vec{p}_{\overline{Q}k})\Big)\end{aligned}$$

Correlated pairs: $j=k$

$$\begin{aligned}\frac{d\sigma^{pA\to Q\overline{Q}+X}_{\rm corr}}{d^3\vec{p}_Q d^3\vec{p}_{\overline{Q}}} &= \int d^2\mathbf{b}\sum_{N=1}^{\infty}\frac{\overline{N}^N_{Q\overline{Q}}(\mathbf{b})e^{-\overline{N}_{Q\overline{Q}}(\mathbf{b})}}{N!}N\frac{1}{\tilde{\sigma}^{Q\overline{Q}}}\frac{d\tilde{\sigma}^{Q\overline{Q}}}{d^3\vec{p}_Q d^3\vec{p}_{\overline{Q}}}\\ &= \int d^2\mathbf{b}\,T_A(\mathbf{b})\frac{d\tilde{\sigma}^{Q\overline{Q}}}{d^3\vec{p}_Q d^3\vec{p}_{\overline{Q}}} = A\frac{d\tilde{\sigma}^{Q\overline{Q}}}{d^3\vec{p}_Q d^3\vec{p}_{\overline{Q}}}\end{aligned}$$

Uncorrelated pairs: $j\neq k$

$$\begin{aligned}\frac{d\sigma^{pA\to Q\overline{Q}+X}_{\rm uncorr}}{d^3\vec{p}_Q d^3\vec{p}_{\overline{Q}}} &= \int d^2\mathbf{b}\sum_{N=1}^{\infty}\frac{\overline{N}^N_{Q\overline{Q}}(\mathbf{b})e^{-\overline{N}_{Q\overline{Q}}(\mathbf{b})}}{N!}N(N-1)\frac{1}{\tilde{\sigma}^{Q\overline{Q}}}\frac{d\tilde{\sigma}^{Q\overline{Q}}}{d^3\vec{p}_Q}\frac{1}{\tilde{\sigma}^{Q\overline{Q}}}\frac{d\tilde{\sigma}^{Q\overline{Q}}}{d^3\vec{p}_{\overline{Q}}}\\ &= \int d^2\mathbf{b}\,T_A^2(\mathbf{b})\frac{d\tilde{\sigma}^{Q\overline{Q}}}{d^3\vec{p}_Q}\frac{d\tilde{\sigma}^{Q\overline{Q}}}{d^3\vec{p}_{\overline{Q}}} = \frac{A^2}{\pi R_A^2}\frac{d\tilde{\sigma}^{Q\overline{Q}}}{d^3\vec{p}_Q}\frac{d\tilde{\sigma}^{Q\overline{Q}}}{d^3\vec{p}_{\overline{Q}}}\end{aligned}$$

Uncorrelated Pairs a Minimal Contribution to Total $D\overline{D}$ Decays at RHIC

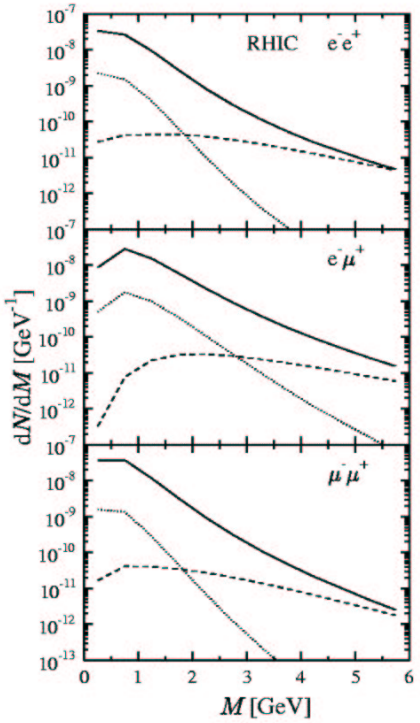

Figure 11: Correlated (solid) and uncorrelated (dashed) $D\overline{D}$ and correlated $B\overline{B}$ (dot-dashed) decays in the e^+e^-, $e^\pm\mu^\mp$, and $\mu^+\mu^-$ lepton pair channels. If a K factor was included, it would enter linearly for the correlated pairs and quadratically for the uncorrelated pairs. [K.J. Eskola, V.J. Kolhinen and R.V., Nucl. Phys. **A696** (2001) 729.]

Shadowing Parameterizations

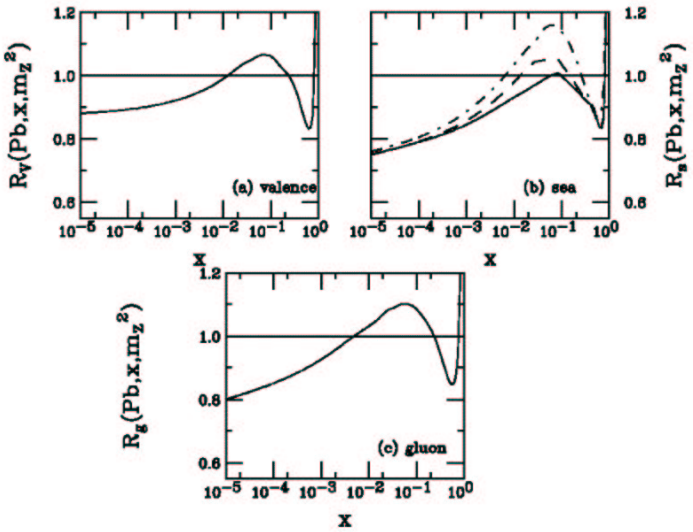

Figure 2: The EKS98 shadowing parameterization evaluated at $Q = m_Z$. Valence shadowing is shown in (a), sea quark shadowing is shown in (b) for $\overline{u} = \overline{d}$ (solid), $\overline{s}$ (dashed) and $\overline{c}$ (dot-dashed), and gluon shadowing is shown in (c).

Shadowing in Gauge Boson Production

Production of a vector particle with mass m_V at scale Q at next-to-leading order

$$\begin{aligned}\frac{1}{AB}\frac{d\sigma^V_{AB}}{dy} &= \int dz\,dz'dx_1dx_2dx\delta\Big(\frac{m_V^2}{s}-xx_1x_2\Big)\delta\Big(y-\frac{1}{2}\ln\Big(\frac{x_1}{x_2}\Big)\Big)\\ &\times\Big\{\sum_{i,j\in Q,\overline{Q}}H^V_{ij}C^{\rm ii}(q_i,\overline{q}_j)\Delta_{q\overline{q}}(x)F^A_{q_i}(x_1,Q^2)F^B_{\overline{q}_j}(x_2,Q^2)\\ &+\sum_{i,k\in Q,\overline{Q}}H^V_{ij}C^{\rm if}(q_i,q_k)\Delta_{qg}(x)\Big[F^A_{q_i}(x_1,Q^2)F^B_g(x_2,Q^2)\\ &+F^A_g(x_1,Q^2)F^B_{q_j}(x_2,Q^2)\Big]\Big\}\,,\end{aligned}$$

$$\begin{aligned}H^{Z^0}_{ij} &= \frac{8\pi}{3}\frac{G_F}{\sqrt{2}}[(g^i_V)^2+(g^i_A)^2]\frac{m_Z^2}{s}\\ H^{W^\pm}_{ij} &= \frac{2\pi}{3}\frac{G_F}{\sqrt{2}}\frac{m_W^2}{s}\\ G_F &= 1.16639\times10^{-5}\ {\rm GeV}^{-2}\end{aligned}$$

Shadowing effects clearest in rapidity distributions

We use MRST HO central gluon and set $Q=m_V$

To study scale dependence, we also take $Q=m_V/2$ and $2m_V$

Universal $\mathcal{O}(\alpha_s\alpha^2)$ Corrections to the LO $\mathcal{O}(\alpha^2)$ Cross Sections

$$\begin{aligned}\Delta_{q\overline{q}}(x) &= \delta(1-x)+\frac{\alpha_s}{3\pi}\Big\{-4(1+x)\ln\Big(\frac{Q^2}{m^2}\Big)-8(1+x)\ln(1-x)-4\frac{1+x^2}{1-x}\ln x\\ &+\delta(1-x)\Big[6\ln\Big(\frac{Q^2}{m^2}\Big)+8\zeta(2)-16\Big]+8\mathcal{D}_0(x)\ln\Big(\frac{Q^2}{m^2}\Big)+16\mathcal{D}_1(x)\Big\}\,.\end{aligned}$$

$$\mathcal{D}_i(x)=\delta(1-x)\frac{\ln^{i+1}(1-x)}{i+1}+\theta(1-\delta-x)\frac{\ln^i(1-x)}{1-x}$$

$$\int_a^1 dx\,f(x)\Big[\frac{\ln(1-x)}{1-x}\Big]_+=\int_a^1 dx\frac{f(x)-f(1)}{1-x}\ln(1-x)+\frac{1}{2}f(1)\ln^2(1-x)$$

$$\Delta_{qg}(x)=\frac{\alpha_s}{8\pi}\Big\{2(1+2x^2-2x)\ln\Big(\frac{(1-x)^2Q^2}{xm^2}\Big)+1-7x^2+6x\Big\}\,.$$

$(g^i_V)^2+(g^i_A)^2=(1/8)(1-4|e_i|x_W+8e_i^2x_W^2)$
where $x_W=\sin^2\theta_W=1-m_W^2/m_Z^2$

Z^0 Production: Convolution of Shadowing Functions with Parton Densities

$q\overline{q} \to Z^0 X$

$$\sum_{i,j\in Q\overline{Q}} S^i(A,x_1)S^j(B,x_2)f_{q_i}^N(x_1,Q^2)f_{\overline{q}_j}^N(x_2,Q^2)C^{i\overline{i}}(q_i,\overline{q}_j)[(g_V^i)^2+(g_A^i)^2]$$
$$= \frac{1}{8}[1-\frac{8}{3}x_W+\frac{32}{9}x_W^2]\left(S^u(A,x_1)S^{\overline{u}}(B,x_2)\left\{Z_Af_u^p(x_1,Q^2)+N_Af_u^n(x_1,Q^2)\right\}\right.$$
$$\times\left\{Z_Bf_{\overline{u}}^p(x_2,Q^2)+N_Bf_{\overline{u}}^n(x_2,Q^2)\right\}+2ABS^c(A,x_1)S^{\overline{c}}(B,x_2)f_c^p(x_1,Q^2)f_{\overline{c}}^p(x_2,Q^2)\Big)$$
$$+\frac{1}{8}[1-\frac{4}{3}x_W+\frac{8}{9}x_W^2]\left(S^d(A,x_1)S^{\overline{d}}(B,x_2)\left\{Z_Af_d^p(x_1,Q^2)+N_Af_d^n(x_1,Q^2)\right\}\right.$$
$$\times\left\{Z_Bf_{\overline{d}}^p(x_2,Q^2)+N_Bf_{\overline{d}}^n(x_2,Q^2)\right\}+2ABS^s(A,x_1)S^{\overline{s}}(B,x_2)f_s^p(x_1,Q^2)f_{\overline{s}}^p(x_2,Q^2)\Big)$$
$$+[x_1\leftrightarrow x_2,A\leftrightarrow B]\,.$$

$q(\overline{q})g \to Z^0 X$

$$\sum_{i,k\in Q\overline{Q}}\Big(S^i(A,x_1)S^g(B,x_2)f_{q_i}^N(x_1,Q^2)f_g^N(x_2,Q^2)$$
$$+[x_1\leftrightarrow x_2,A\leftrightarrow B]\Big)C^{ik}(q_i,q_k)[(g_V^i)^2+(g_A^i)^2]$$
$$= BS^g(B,x_2)f_g^p(x_2,Q^2)$$
$$\times\Big\{\frac{1}{8}[1-\frac{8}{3}x_W+\frac{32}{9}x_W^2]\left(S^u(A,x_1)\left\{Z_Af_u^p(x_1,Q^2)+N_Af_u^n(x_1,Q^2)\right\}\right.$$
$$+S^{\overline{u}}(A,x_1)\left\{Z_Bf_{\overline{u}}^p(x_2,Q^2)+N_Bf_{\overline{u}}^n(x_2,Q^2)\right\}+2AS^c(A,x_1)f_c^p(x_1,Q^2)\Big)$$
$$+\frac{1}{8}[1-\frac{4}{3}x_W+\frac{8}{9}x_W^2]\left(S^d(A,x_1)\left\{Z_Af_d^p(x_1,Q^2)+N_Af_d^n(x_1,Q^2)\right\}\right.$$
$$+\left.S^{\overline{d}}(A,x_1)\left\{Z_Bf_{\overline{d}}^p(x_2,Q^2)+N_Bf_{\overline{d}}^n(x_2,Q^2)\right\}+2AS^s(A,x_1)f_s^p(x_1,Q^2)\right)\Big\}$$
$$+[x_1\leftrightarrow x_2,A\leftrightarrow B]\,.$$

Z^0 Distributions in pp Collisions at 5.5 and 14 TeV

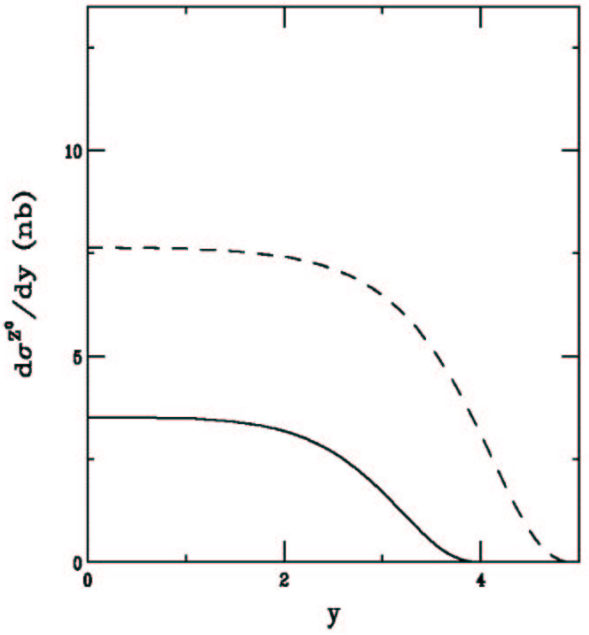

Figure 6: The Z^0 rapidity distributions in pp collisions at 5.5 (solid) and 14 TeV (dashed), calculated with the MRST HO distributions.

Z^0 Distributions in Pbp and pPb Collisions at 5.5 TeV

Small isospin effects on Z^0 production

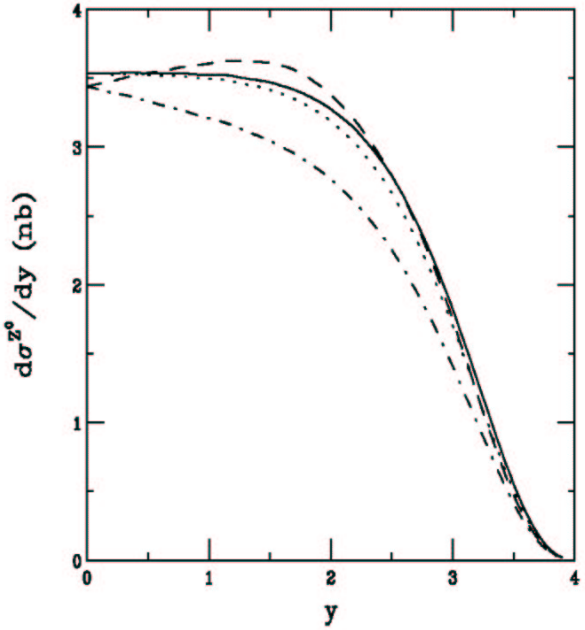

Figure 8: The Z^0 rapidity distributions in Pbp and pPb collisions at 5.5 TeV, calculated with the MRST HO distributions. The solid and dashed curves show the results without and with shadowing respectively with the Pb nucleus coming from the left. The dotted and dashed curves give the results without and with shadowing for the proton coming from the left.

Shadowing Effects on Z^0 Production in Pbp and pPb Collisions at 5.5 TeV

In Pbp collisions, x_1 is in nucleus, x_1 increases with y into antishadowing and Fermi motion region, ratio increases

In pPb collisions, x_2 in nucleus, goes into shadowing region, ratio decreases

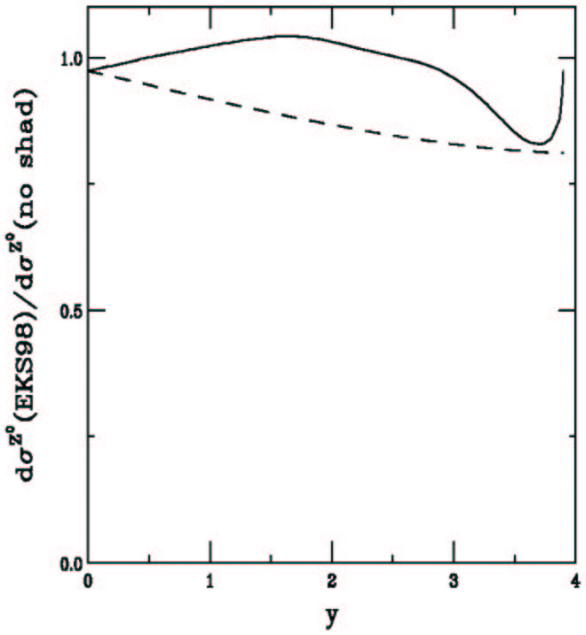

Figure 9: Ratios of shadowed to unshadowed Z^0 rapidity distributions in Pbp (solid) and pPb (dashed) collisions at 5.5 TeV.

Model Dependence of Shadowing on Z^0 Production in Pbp Collisions

Compare EKS98, HPC, and HKM (LO only)

Stronger HKM antishadowing at large y because of increasing q_S with x_1 and weaker q_V shadowing

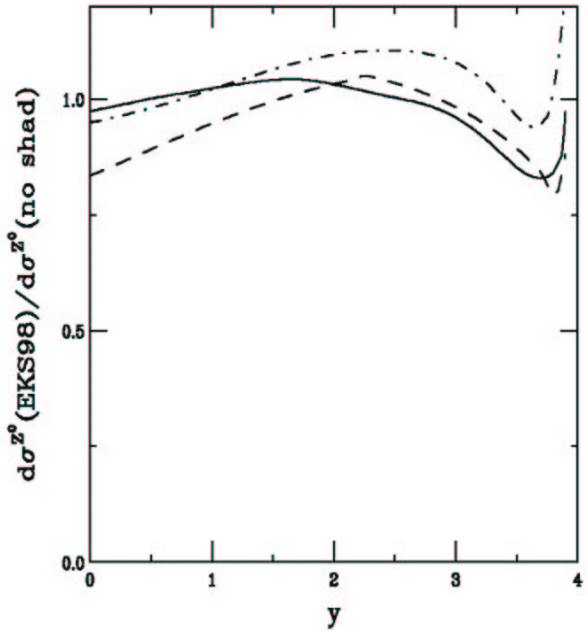

Figure 10: Ratios of shadowed to unshadowed Z^0 rapidity distributions in Pbp collisions at 5.5 TeV using the EKS98 (solid), HPC (dashed) and HKM (dot-dashed) shadowing parameterizations.

Model Dependence of Shadowing on Z^0 Production in pPb Collisions

HKM shadowing almost independent of x_2 due to weaker sea quark shadowing

HPC has stronger shadowing at low x_2 because it has no Q^2 evolution

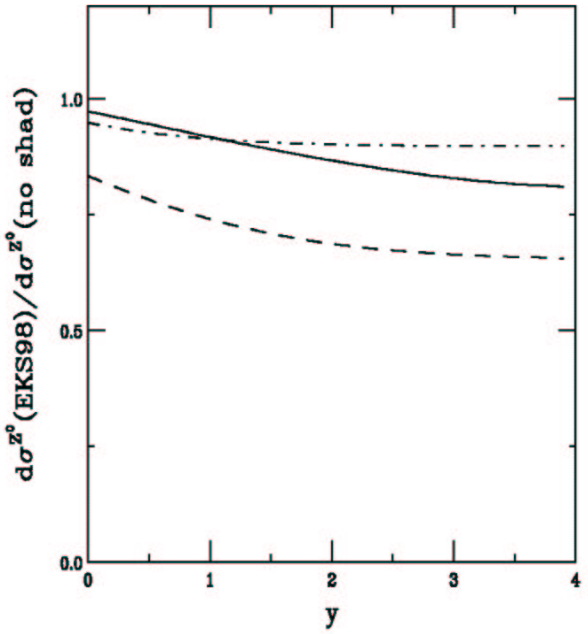

Figure 11: Ratios of shadowed to unshadowed Z^0 rapidity distributions in pPb collisions at 5.5 TeV using the EKS98 (solid), HPC (dashed) and HKM (dot-dashed) shadowing parameterizations.

Scale Dependence of Shadowing on Z^0 Production in Pbp Collisions

Results above $Q = 2m_V$ are unreliable because EKS98 only evolved to 100 GeV

Decreasing scale increases shadowing because evolution reduced

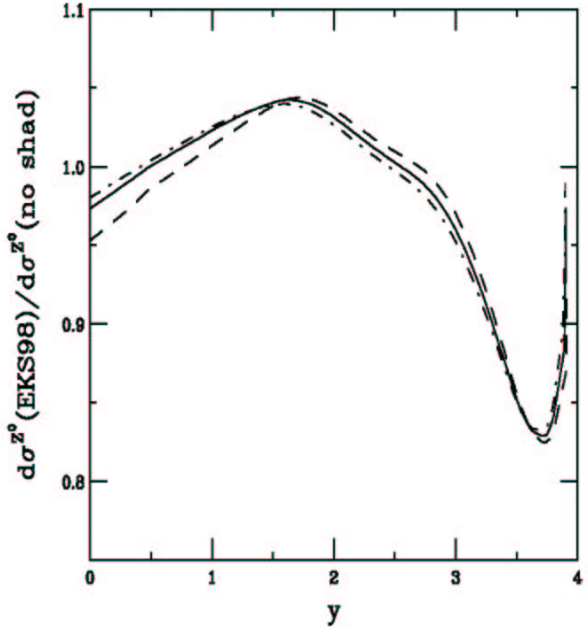

Figure 12: Ratios of shadowed to unshadowed Z^0 rapidity distributions in Pbp collisions at 5.5 TeV using the EKS98 parameterization. The curves show $Q = m_V$ (solid), $m_V/2$ (dashed) and $2m_V$.

Scale Dependence of Shadowing on Z^0 Production in pPb Collisions

Evolution of shadowing stronger when Pb is target because shadowing affects sea quarks more strongly at low x_2

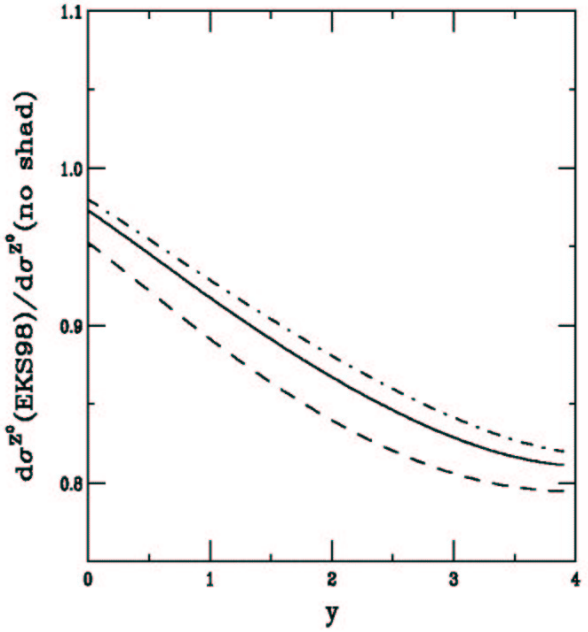

Figure 13: Ratios of shadowed to unshadowed Z^0 rapidity distributions in pPb collisions at 5.5 TeV using the EKS98 parameterization. The curves show $Q = m_V$ (solid), $m_V/2$ (dashed) and $2m_V$.

Z^0 Production Ratios Pbp/pp and pPb/pp at 5.5 TeV

Ratios without shadowing show isospin effect, small for Z^0

Thus ratios with shadowing look like shadowed/unshadowed ratios

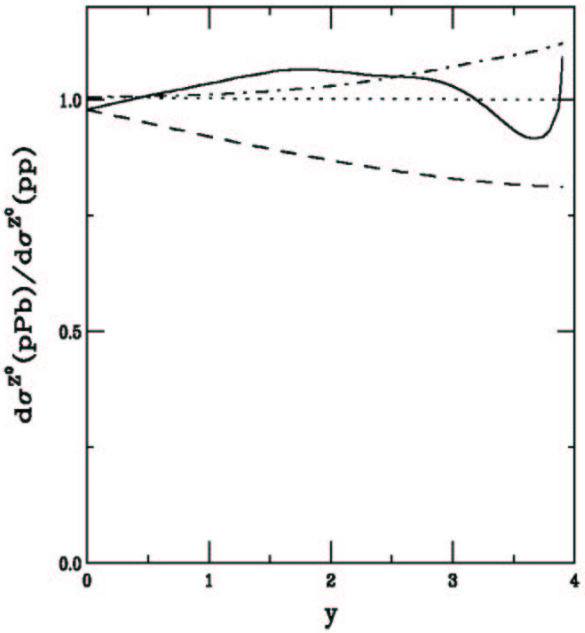

Figure 14: The ratios of Pbp/pp with (solid) and without (dot-dashed) shadowing and pPb/pp with (dashed) and without (dotted) shadowing at 5.5 TeV.

W^+ Production: Convolution of Shadowing Functions with Parton Densities

$q\bar{q} \to W^+X$

$$\sum_{i,j\in Q,\bar{Q}} S^i(A,x_1)S^j(B,x_2)f_{q_i}^N(x_1,Q^2)f_{\bar{q}_j}^N(x_2,Q^2)C^{ij}(q_i,\bar{q}_j)$$
$$= \cos^2\theta_C\left(S^u(A,x_1)S^{\bar{d}}(B,x_2)\left\{Z_A f_u^p(x_1,Q^2)+N_A f_u^n(x_1,Q^2)\right\}\right.$$
$$\times\left\{Z_B f_{\bar{d}}^p(x_2,Q^2)+N_B f_{\bar{d}}^n(x_2,Q^2)\right\}+ABS^{\bar{s}}(A,x_1)S^c(B,x_2)f_{\bar{s}}^p(x_1,Q^2)f_c^p(x_2,Q^2)\Big)$$
$$+\sin^2\theta_C\left(S^u(A,x_1)S^{\bar{s}}(B,x_2)\left\{Z_A f_u^p(x_1,Q^2)+N_A f_u^n(x_1,Q^2)\right\}Bf_{\bar{s}}^p(x_2,Q^2)\right.$$
$$\left.+S^{\bar{d}}(A,x_1)S^c(B,x_2)\left\{Z_A f_{\bar{d}}^p(x_1,Q^2)+N_A f_{\bar{d}}^n(x_1,Q^2)\right\}Bf_c^p(x_2,Q^2)\right)\Big\}$$
$$+[x_1\leftrightarrow x_2, A\leftrightarrow B]\,.$$

$q(\bar{q})g \to W^+X$

$$\sum_{i,k\in Q\bar{Q}}\Big(S^i(A,x_1)S^g(B,x_2)f_{q_i}^N(x_1,Q^2)f_g^N(x_2,Q^2)+[x_1\leftrightarrow x_2, A\leftrightarrow B]\Big)C^{ik}(q_i,q_k)$$
$$= BS^g(B,x_2)f_g^p(x_2,Q^2)\Big[S^u(A,x_1)\left\{Z_A f_u^p(x_1,Q^2)+N_A f_u^n(x_1,Q^2)\right\}$$
$$+S^{\bar{d}}(A,x_1)\left\{Z_B f_{\bar{d}}^p(x_2,Q^2)+N_B f_{\bar{d}}^n(x_2,Q^2)\right\}+A\left\{S^{\bar{s}}(A,x_1)f_{\bar{s}}^p(x_1,Q^2)+S^c(A,x_1)f_c^p(\right.$$
$$+[x_1\leftrightarrow x_2, A\leftrightarrow B]\,.$$

W^+ Distributions in pp Collisions at 5.5 and 14 TeV

pp cross sections increase with y due to dominance of $u_p(x_1)\overline{d}_p(x_2)$ contribution, $u_{Vp}(x_1)$ goes up with x_1 while $\overline{d}_p(x_2)$ goes up when x_2 decreases, peak at same point as in u_V distribution

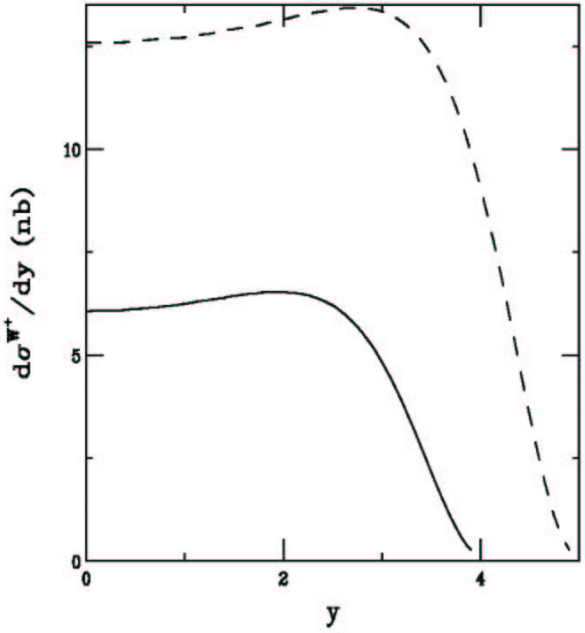

Figure 15: The W^+ rapidity distributions in pp collisions at 5.5 (solid) and 14 TeV (dashed), calculated with the MRST HO distributions.

W^+ Distributions in Pbp and pPb Collisions at 5.5 TeV

Pbp neutron excess wipes out rise with y

pPb, $(N/A)d_p(x_1)\overline{d}_p(x_2)$ enhances pA because $\overline{d} > \overline{u}$

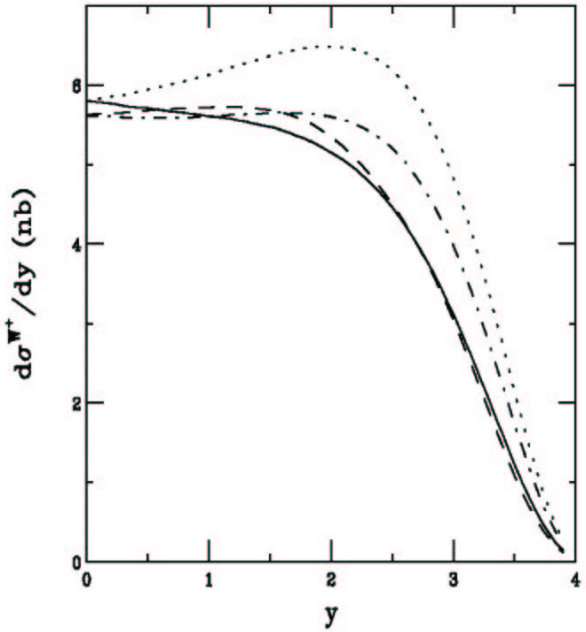

Figure 17: The W^+ rapidity distributions in Pbp and pPb collisions at 5.5 TeV, calculated with the MRST HO distributions. The solid and dashed curves show the results without and with shadowing respectively with the Pb nucleus coming from the left. The dotted and dashed curves give the results without and with shadowing for the proton coming from the left.

W^+ Production Ratios Pbp/pp and pPb/pp at 5.5 TeV

Neutron excess depletes Pbp/pp

pPb/pp without shadowing shows a rise due to extra neutrons in Pb (x_2)

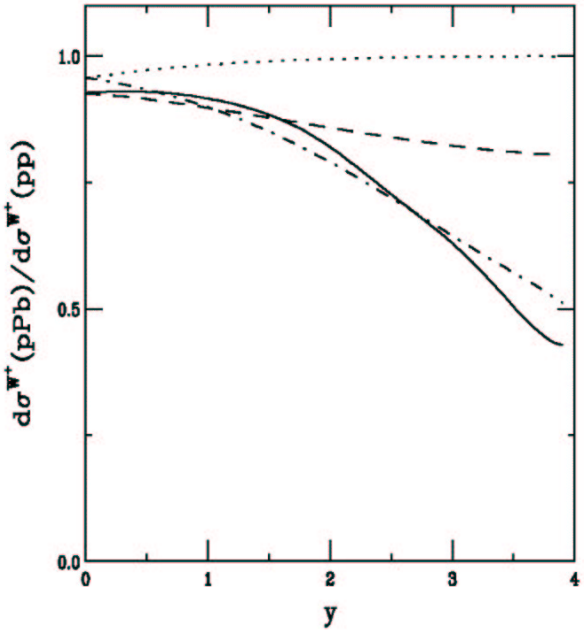

Figure 19: The ratios of Pbp/pp with (solid) and without (dot-dashed) shadowing and pPb/pp with (dashed) and without (dotted) shadowing at 5.5 TeV.

W^- Production: Convolution of Shadowing Functions with Parton Densities

$q\overline{q} \to W^-X$

$$\sum_{i,j\in Q\overline{Q}} S^i(A,x_1)S^j(B,x_2)f_{q_i}^N(x_1,Q^2)f_{\overline{q}_j}^N(x_2,Q^2)C^{i\overline{i}}(q_i,\overline{q}_j)$$
$$= \cos^2\theta_C\left(S^{\overline{u}}(A,x_1)S^d(B,x_2)\left\{Z_A f_{\overline{u}}^p(x_1,Q^2)+N_A f_{\overline{u}}^n(x_1,Q^2)\right\}\right.$$
$$\times\left\{Z_B f_d^p(x_2,Q^2)+N_B f_d^n(x_2,Q^2)\right\}+ABS^s(A,x_1)S^{\overline{c}}(B,x_2)f_s^p(x_1,Q^2)f_{\overline{c}}^p(x_2,Q^2))$$
$$+\sin^2\theta_C\left(S^{\overline{u}}(A,x_1)S^s(B,x_2)\left\{Z_A f_{\overline{u}}^p(x_1,Q^2)+N_A f_{\overline{u}}^n(x_1,Q^2)\right\}Bf_s^p(x_2,Q^2)\right.$$
$$\left.+S^d(A,x_1)S^{\overline{c}}(B,x_2)\left\{Z_A f_d^p(x_1,Q^2)+N_A f_d^n(x_1,Q^2)\right\}Bf_{\overline{c}}^p(x_2,Q^2))\right\}$$
$$+[x_1\leftrightarrow x_2, A\leftrightarrow B]\,.$$

$q(\overline{q})g \to W^-X$

$$\sum_{i,k\in Q\overline{Q}}\Big(S^i(A,x_1)S^g(B,x_2)f_{q_i}^N(x_1,Q^2)f_g^N(x_2,Q^2)+[x_1\leftrightarrow x_2, A\leftrightarrow B]\Big)C^{ik}(q_i,q_k)$$
$$= BS^g(B,x_2)f_g^p(x_2,Q^2)\Big[S^{\overline{u}}(A,x_1)\left\{Z_A f_{\overline{u}}^p(x_1,Q^2)+N_A f_{\overline{u}}^n(x_1,Q^2)\right\}$$
$$+S^d(A,x_1)\left\{Z_B f_d^p(x_2,Q^2)+N_B f_d^n(x_2,Q^2)\right\}+A\left\{S^s(A,x_1)f_s^p(x_1,Q^2)+S^{\overline{c}}(A,x_1)f_{\overline{c}}^p(\right.$$
$$+[x_1\leftrightarrow x_2, A\leftrightarrow B]\,.$$

W^- Distributions in pp Collisions at 5.5 and 14 TeV

W^- decreases with y because valence d has smaller x

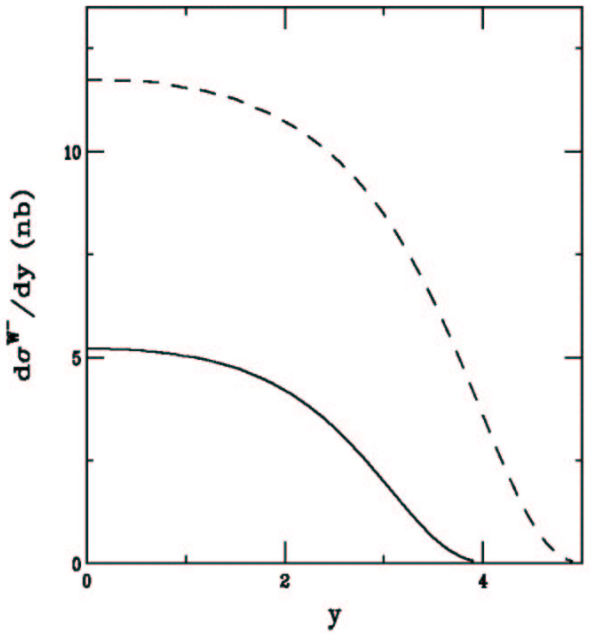

Figure 20: The W^- rapidity distributions in pp collisions at 5.5 (solid) and 14 TeV (dashed), calculated with the MRST HO distributions.

W^- Distributions in Pbp and pPb Collisions at 5.5 TeV

Neutron excess in Pb enhances Pbp at large y ($(N/A)u_p(x_1)\overline{u}_p(x_2)$)

pPb has smaller isospin effect

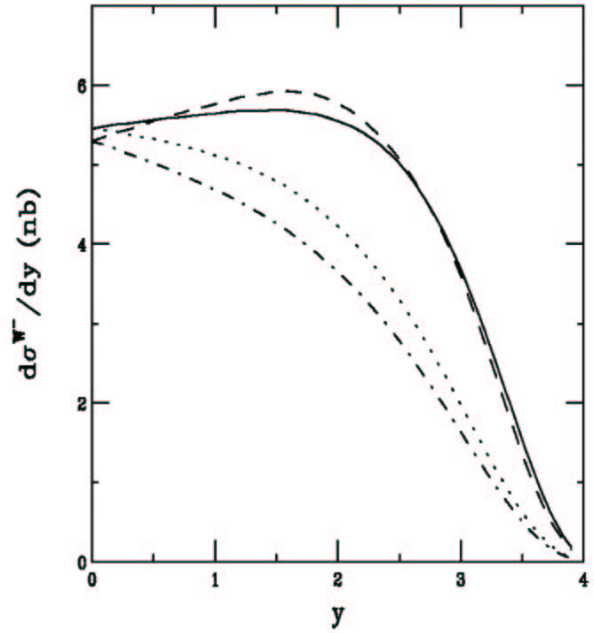

Figure 22: The W^- rapidity distributions in Pbp and pPb collisions at 5.5 TeV, calculated with the MRST HO distributions. The solid and dashed curves show the results without and with shadowing respectively with the Pb nucleus coming from the left. The dotted and dashed curves give the results without and with shadowing for the proton coming from the left.

W^- Production Ratios Pbp/pp and pPb/pp at 5.5 TeV

Pbp/pp enhanced by neutron excess

pPb/pp shows small depletion with y

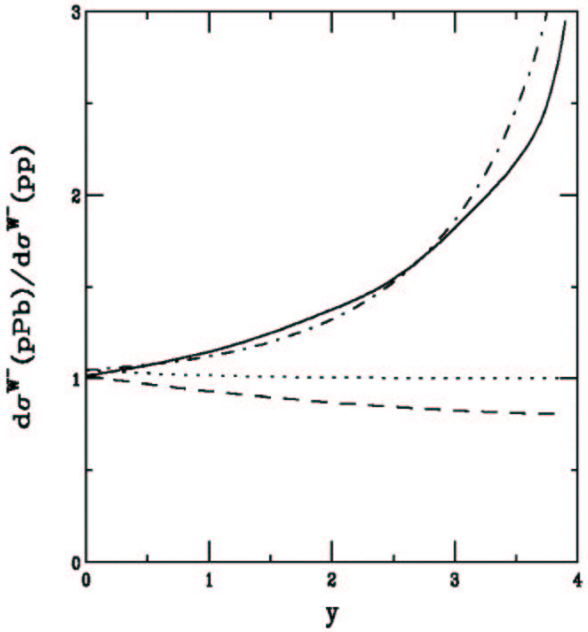

Figure 24: The ratios of Pbp/pp with (solid) and without (dot-dashed) shadowing and pPb/pp with (dashed) and without (dotted) shadowing at 5.5 TeV.